

Research Article

Zn-M-CO₃ Layered Double Hydroxides (M=Fe, Cr, or Al): Synthesis, Characterization, and Removal of Aqueous Indigo Carmine

Salima Bouteraa^{1*}, Fatiha Boukraa Djellal Saiah¹, Sarah Hamouda^{1,2},
Nourredine Bettahar¹

¹Laboratory of Inorganic Materials Chemistry and Application, University of Sciences and Technology of Oran - USTO BP. 1505 Oran, Algeria.

²Center of Scientific Research and Technique in Physicochemical Analysis (CRAPC), Bou-Smail, Tipaza, Algeria.

Received: 7th June 2019; Revised: 23rd August 2019; Accepted: 27th August 2019;
Available online: 28th February 2020; Published regularly: April 2020

Abstract

In this approach, Zn-M⁺³ layered double hydroxides (LDHs) with M⁺³ = Fe, Cr, or Al were synthesized by the coprecipitation method from the aqueous solution at a constant solution pH. The as-synthesized samples were characterized by XRD analysis, FTIR spectra, BET techniques and simultaneous thermogravimetric-differential scanning calorimetry (TGA/DSC). XRD analysis showed that Zn-Fe-CO₃ had the greatest lattices parameters. BET surface area of Zn-Fe-CO₃ was calculated as 52.24 m².g⁻¹ and was higher than Zn-Cr-CO₃ and Zn-Al-CO₃ with 46.70 and 49.99 m².g⁻¹, respectively. The FTIR spectra clearly confirmed the presence of carbonate anions in the structure of the LDHs. Adsorption experiments for Indigo Carmine (IC), as the main model organic pollutant in this study from aqueous solution onto synthesized samples were carried out in terms of solution pH, contact time and initial dye concentration. Experimental results indicate that the capacity of dye uptake augmented rapidly within the first 15, 40, and 55 minutes for Zn-Fe-CO₃, Zn-Cr-CO₃ and Zn-Al-CO₃ respectively and then stayed practically the same regardless of the concentration. Adsorption kinetics studies revealed that the adsorption process followed pseudo-second order kinetics model instead of a pseudo-first-order model. The adsorption isotherm data follow the Langmuir equation in which parameters are calculated. The maximum Langmuir monolayer adsorption capacities were 94.87, 21.79, and 66.71 mg.g⁻¹ for Zn-Fe-CO₃, Zn-Cr-CO₃, and Zn-Al-CO₃, respectively. The adsorption capacities were slightly influenced by the pH variations from 5 to 10, showing the advantage of using these materials in water treatments in a wide pH range. Finally, the IC removal is proven by the presence of IC functional groups in IR spectra and thermograms. TGA/DSC of Zn-Fe-CO₃ obtained after removal of IC indicate that the LDHs stabilizes IC and delays the combustion of adsorbed molecules. Copyright © 2020 BCREC Group. All rights reserved

Keywords: Layered Double Hydroxide; Coprecipitation; Characterization; Adsorption; Indigo Carmine

How to Cite: Bouteraa, S., Saiah, F.B.D., Hamouda, S., Bettahar, N. (2020). Zn-M-CO₃ Layered Double Hydroxides (M=Fe, Cr, or Al): Synthesis, Characterization, and Removal of Aqueous Indigo Carmine. *Bulletin of Chemical Reaction Engineering & Catalysis*, 15(1): 43-54 (doi:10.9767/bcrec.15.1.5053.43-54)

Permalink/DOI: <https://doi.org/10.9767/bcrec.15.1.5053.43-54>

1. Introduction

Dyes are widely used in many industries. Large quantities of dye effluents are discharged from the dyeing process causing serious environmental problems resulting from the water

pollution. Most of these dyes are toxic, mutagenic and carcinogenic [1-4]. The consequences can be severe for water resources if the man primarily responsible for this pollution would not intervene to solve this problem. For this, there must be means, both technical and legal, sufficient to fight this scourge and protect the quality of water resources. Indigo carmine is commonly one of anionic dyes, it was released by many indus-

* Corresponding Author.

E-mail: salima.bouteraa@univ-usto.dz (S. Bouteraa);
Telp: +213 782 922 462

tries, such as textile, papers and plastics processors, and caused serious pollution in water bodies [5]. Due to its symmetrical structure and stable properties, it is difficult to be oxidized and cracked. Recently, the removal of dye based toxic and carcinogenic pollutants from the industrial wastewater has been of interest in numerous studies [6-9].

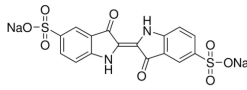
Many advanced researches have been focused on different methods for dye removal from wastewaters such as biological degradation [10], photodegradation [11], coagulation [12], membrane filtration [12], reverse osmosis [14], adsorption [6,9], or the synergic treatment using different methods. Therefore, adsorption was the treatment economic solution and has been widely studied for a high-efficiency [15].

Recent studies showed that the use of layered double hydroxides for the retention of organic anions has shown very good results [16,17]. LDHs have received considerable attention due to their properties and multiple applications as catalysts [18], sorbents [19-21], ions exchangers [22-24]. The most important class of LDHs or hydrotalcite-like compounds can be represented by the general formula $[M^{2+}_{1-x}M^{3+}_x(OH)_2]^{x+} [A^{n-}_{x/n}.mH_2O]$ where M^{2+} and M^{3+} are divalent (Zn^{2+} , Mg^{2+} , Fe^{2+} , Co^{2+} , Cu^{2+} , Ni^{2+}) and trivalent (Fe^{3+} , Cr^{3+} , Al^{3+} , In^{3+} , Mn^{3+} , Ga^{3+}) metal ions, respectively that occupy octahedral sites in the hydroxide layers; A^{n-} is an exchangeable anion (CO_3^{2-} , SO_4^{2-} , NO_3^- , F^- , Cl^-), and x is the ratio of $M^{3+}/(M^{2+}+M^{3+})$ ranges from 0.17 to 0.33. The layers have a brucite-like structure [25], in which the isomorphic substitution of some divalent cations by trivalent ones gives rise to the positive residual charge [26,27], which require the presence of interlayer anions to maintain overall charge neutrality.

The LDHs physicochemical properties are significantly modified by the nature of the divalent ion, trivalent ion and interlayer anion [28,29]; thus, their capacities for the adsorption of pollutants can be altered. The previous studies showed that different kinds of metal cations, i.e. Zn^{2+} , Mg^{2+} and Ni^{2+} influence the crystallinity and the interlayer distance was dependent on ionic radii [30]. It can be assumed that varying in trivalent metal cations, i.e. Fe^{3+} , Cr^{3+} , Al^{3+} would achieve different improved effects on treatment performance of wastewater.

Therefore, the present investigation concerns the synthesis and characterization of $Zn-M^{3+}$ layered double hydroxides (LDHs) with $M^{3+}=Fe, Cr$ or Al with a view to understanding the role of the trivalent cation on the structure, crystallinity, thermal stability and studying their sorption capacity for IC dye, the procedure for the synthesis of $Zn-Fe^{(III)}$ LDHs by using $Fe^{(II)}$ is also described. In one such process, the precipitate from Zn and $Fe^{(II)}$ reagents was oxidized to convert $Fe^{(II)}$ into $Fe^{(III)}$ within the solid framework with a Zn/Fe molar ratio of 1 :1 which has not been discussed before. The samples were characterized by powder XRD, FTIR, BET and TGA/DSC. The resulting materials were then used as adsorbent for removal of Indigo Carmine (Table 1), a highly toxic indigoid class of dye, from aqueous solution. The effects of various parameters on the removal of Indigo Carmine, such as: pH of solution, equilibrium time, and concentration of Indigo Carmine, have been studied in detail to determine the efficiency of these materials under optimized conditions. The localization of the dye in the interlayer space of our samples is studied by infrared spectroscopy (FT-IR) and thermograms. In addition, the Langmuir and Freun-

Table 1. Physical properties and molecular structure of Indigo Carmine [6]

Dye name	Indigo Carmine
Molecular structure	
Chemical formula	$C_{16}H_8N_2Na_2O_8S_2$
Molecular Weight	466.36 g.mol ⁻¹
IUPAC name	3,3'-dioxo-2,2'-bisindolyden-5,5'-disulfonic acid disodium salt
Aspect	Dark blue powder
λ_{max} (nm)	610
Melting	>300 °C
Temperature solubility	10 g.L ⁻¹ (water, 25°C)
Uses	Textile dye

dlich adsorption isotherm models were applied in order to fit the experimental data in linear and nonlinear regression, kinetic models (first-order, pseudo-second-order) have been also investigated. However, to our knowledge, there is no published information about the use of these three materials as adsorbents of IC from water.

2. Materials and Methods

2.1 Materials

All the steps of the synthesis were conducted using distilled water. Synthetic reagents used were at least 98-99 % pure and were supplied by Biochem Chemopharma, Merck for Indigo Carmine (IC) (purity >99%). The Characteristics of organic was used as the model pollutant in evaluation of the adsorption are given in (Table 1). A stock solution of 1000 ppm was prepared by dissolving 1 g of IC in 1 L of distilled water. The solid adsorbent materials were prepared as described in Section 2.2.1.

2.2 Methods

2.2.1 Preparation of LDHs

Zn-M-LDHs with (M= Fe, Cr, or Al) were prepared by well-known co-precipitation method. Co-precipitation method is not only simple and low cost but also produces large scale of products. Typically, 0.05 mole of NaOH and 0.1 mole of Na₂CO₃ were dissolved in 50 mL of deionized water to which 50 mL mixed solution containing 0.1 mole of Zn(NO₃)₂.6H₂O and (0.05 mole of Cr(NO₃)₃.9H₂O or Al(NO₃)₃.9H₂O) with (Zn: M molar ratio = 2:1) was slowly added under vigorous stirring. During the synthesis the pH value was kept constant at 10 by adding suitable amounts of 1 M NaOH solution. The resulting slurries were aged at 343 K for 15 h. After cooling to room temperature; the slurries were centrifuged and washed using deionized water at least eight times to remove free ions. Then the materials were dried at 353 K overnight and the resulting products has a blue-green for Zn-Cr-CO₃ and white for Zn-Al-CO₃.

The preparation of Zn-Fe^(III) Layered double hydroxides using either Fe^(II) or Fe^(III) under a nitrogen atmosphere was reported by Morimoto *et al.* [31]. The product derived from the synthesis employing Fe^(II) was found to transition to a Zn-Fe^(III) layered double hydroxides phase following oxidation process. In contrast, the product obtained with Fe^(III) did not contain a layered double hydroxides phase, but rather consisted of *simonkolleite* and hydrous ferric oxide.

The preparation of Zn-Fe^(III)SO₄LDH using Fe^(II) was also reported by Meng *et al.* [32]. We use a modification of this method to prepare Zn-Fe^(III)-CO₃ LDH by precipitation at constant pH in air using an aqueous solution (50 mL) containing ZnCl₂ and FeCl₂.H₂O (with a Zn/Fe molar ratio of 1:1 and a total metal ion concentration of 1.0 mol.L⁻¹) were slowly added drop wise to 50 mL of distilled water with vigorous stirring at room temperature. During the co-precipitation reaction, the pH in the reaction mixture was maintained at a constant value of 7 by the simultaneous addition of a 1.25 M NaOH solution, during the synthesis the suspension was turquoise blue. The resulting suspension was aged at 313 K for 24 h. The solid products obtained were then centrifuged and washed thoroughly with deionized water and dried at 313 K for 24 h, affording a pale-yellow solid.

2.2.2 Characterizations

Powder X-ray diffraction patterns (XRD) of synthesized LDHs were recorded using Philips PW1820 diffractometer with monochromatic Cu-K α radiation ($\lambda = 1.5418 \text{ \AA}$ at a scan speed of 0.02°/s) over a 2θ range of 5-70°. Identifications of the crystalline phases were done by comparison with the JCPDS files [33]. The incorporation or not of ionic liquid in the as-synthesized materials is confirmed by infrared FTIR spectroscopy. The FTIR spectra are recorded in the range of 4000-400 cm⁻¹ by using KBr pellets technique in a Perkin Elmer FTIR 2000 spectrometer. Specific surface area was measured in a Quantachrome Instruments Nova 1000e surface analyzer by nitrogen adsorption N₂ (77.4 K) after degassing the sample in a vacuum by flowing nitrogen overnight at 100 °C. The surface areas were determined by applying (Brunauer-Emmet-Teller, BET) method in the nitrogen adsorption data. The pore diameter and the pore size distribution were determined by the BJH method [34]. Thermogravimetric/Differential Scanning Calorimetry (TG/DSC) of [Zn-Fe-CO₃], [Zn-Fe-IC], and for pure IC was carried out using LIN-SEIS.STA.PT 1600.ATG-DSC equipment, in the temperature range between 20 and 1200 °C at a heating rate of 10 °C.min⁻¹ in air.

2.2.3 Batch reactor experiments

A dye stock solution of 1000 ppm was prepared by dissolving 1 g of IC in 1 L of distilled water, serial dilutions were made by diluting the dye stock solution in accurate proportions to the desired concentrations from 10 to 200

ppm. For the analysis of aqueous solutions, a pH meter Hanna microprocessor is used for pH measurements. UV-visible spectroscopy is used to determine the amount of residual IC dye in solutions. Experiments are carried out with a UV-Visible "Optizen 2120" spectrometer", the acquisition of UV-Visible spectra is performed through software "Optizen View". The equilibrium batch adsorption studies were accomplished by taken (0.06 g) of each LDH constant and exposing to 20 mL of IC dye solutions in 120 mL amber bottle. The mixtures obtained are magnetically stirred at room temperature. For the pH effect study, the initial pH of the dye solutions was set to different values, from 5 to 10, by adding 1 M HCl or 1M NaOH solutions at a pre-determined concentration of IC for 24 h. For kinetics studies, at given adsorbent dosage and concentration of IC by varying the contact time from 5 to 120 min, they were then stirred under constant speed at room temperature and natural pH, samples were taken until the equilibrium was established. Isotherms experiments were accomplished at optimum time, where 60 mg of adsorbent was added to 20 mL of dye solution with different concentrations, from 10 to 200 mg/solution. After each adsorption experiment was completed, the

solid phase was separated from the liquid phase by centrifugation at 3000 rpm for 10 min. The residual concentrations were determined from UV-Vis characteristics at a maximum absorption wavelength of 610 nm.

In all cases, amounts, Q_e , of IC dye removed by the adsorbent in each flask and the efficiency of adsorption (or removal), R , are determined by the following mass balance Equations (1,2):

$$Q_e = (C_i - C_e) \frac{V}{m} \quad (1)$$

$$R\% = \frac{C_i - C_e}{C_i} * 100\% \quad (2)$$

where, Q_e is the adsorbed amount of dye per gram of adsorbent (mg.g^{-1}), R is the efficiency of adsorption (%), C_i and C_e are initial and equilibrium concentrations in mg.L^{-1} , m is the mass of adsorbent in grams and V is the volume of solution.

Due to the inherent bias resulting from linearization of the isotherm models, the non-linear regression Root Mean Square Error (RMSE), the Chi-Squares (χ^2), and normalized standard deviation (Δq) test methods are employed as criterion for the quality of fitting using Equations (3), (4), and (5), respectively.

$$RMSE = \sqrt{\frac{\sum_{i=1}^n (q_{e,\text{exp}} - q_{e,\text{cal}})^2}{n}} \quad (3)$$

$$\chi^2 = \sum_{i=1}^n \frac{(q_{e,\text{exp}} - q_{e,\text{cal}})^2}{q_{e,\text{cal}}} \quad (4)$$

$$\Delta q = \sqrt{\frac{\sum_{i=1}^n \left[\frac{(q_{e,\text{exp}} - q_{e,\text{cal}})}{q_{e,\text{exp}}} \right]^2}{n-1}} \quad (5)$$

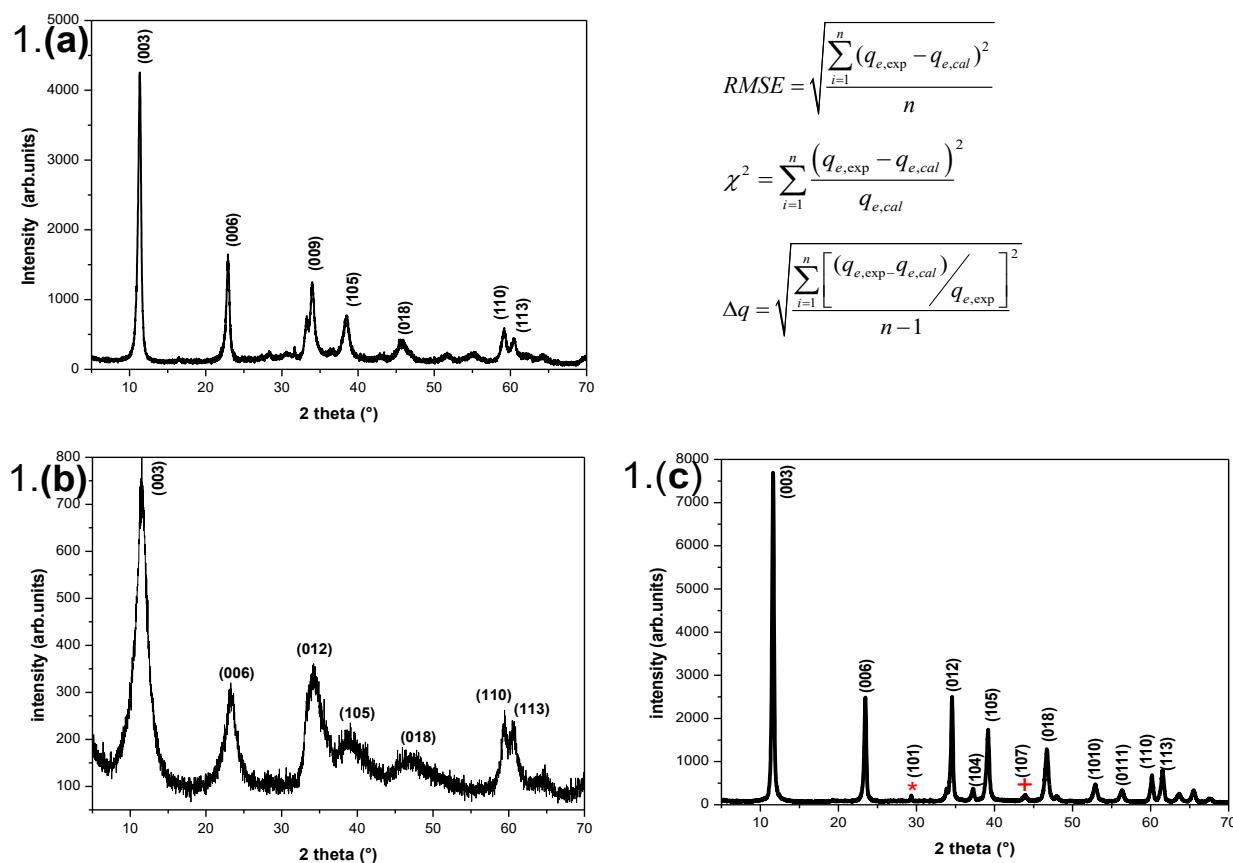


Figure 1. XRD patterns of: (a) Zn-Fe-CO₃, (b) Zn-Cr-CO₃, and (c) Zn-Al-CO₃, (*) Zn(OH)₂ and (+) Al(OH)₃

where, $q_{e,exp}$ and $q_{e,cal}$ are, respectively, the experimental and calculated adsorption capacities as calculated from the model ($\text{mg}\cdot\text{g}^{-1}$), and n is the number of experimental data points. Smaller values correspond to better curve fitting.

3. Results and Discussion

3.1 Characterization of Materials

3.1.1 XRD analysis

The XRD patterns of the three LDHs are displayed in Figure 1, exhibit the characteristic reflections of layered double hydroxides [35]. The XRD pattern consists of both sharp and symmetrical peaks at low 2θ , such as: (003), (006), (012), (009) with some asymmetrical peaks at high angle, the values of their positions give the values of $d_{(hkl)}$. The d_{003} crystal planes with basal spacing was observed at 7.52, 7.66 and 7.78 Å for Zn-Al- CO_3 , Zn-Cr- CO_3 , and Zn-Fe- CO_3 , respectively.

The XRD pattern of Zn-Al- CO_3 also showed $\text{Zn}(\text{OH})_2$ and $\text{Al}(\text{OH})_3$ phases impurities, which can be determined by comparison of their characteristic reflection pattern to a reference library of samples. These phases in the sample may be the consequence of poor control of the pH during the synthesis.

The first peak of the doublet close to a 2θ of approximately ($60\text{--}62^\circ$) is due to the orientation

from the (110) planes, and its spacing corresponds to the lattice parameter a , which coincides with the closest M–M distance in the brucite-like layers. The decrease in the intensity for the (110) plane in the order $\text{Zn-Fe-}\text{CO}_3 > \text{Zn-Al-}\text{CO}_3 > \text{Zn-Cr-}\text{CO}_3$ indicates a decrease in crystallinity.

The cell constant c are commonly calculated as $c=3d_{(003)}$, while the a dimension were calculated as twice the position of the (110) peaks ($a= 2d_{(110)}$). The obtained parameters are presented in (Table 2). These observed differences in “ a ” parameters are in agreement with Vegard’s law for solid solutions, which corroborates the inclusion of metal cations into the LDH sheet. The ionic radius of Fe^{+3} (0.645\AA) was greater than ionic radius of Cr^{+3} (0.615\AA) and Al^{+3} (0.53\AA) [36] and agree well with those reported for hydrotalcite-like compounds [30,31,37].

3.1.2 FTIR

FTIR spectra for all the LDHs shown in Figure 2 are characteristic for the hydrotalcite-like structures. The broad and strong band in the frequency range of $3250\text{--}3500\text{ cm}^{-1}$, centered at 3444 , 3430 , and 3386 cm^{-1} for Zn-Fe- CO_3 , Zn-Cr- CO_3 and Zn-Al- CO_3 , respectively are common for all the hydrotalcite type materials corresponding to the asymmetric and symmetric stretching mode vibration of OH

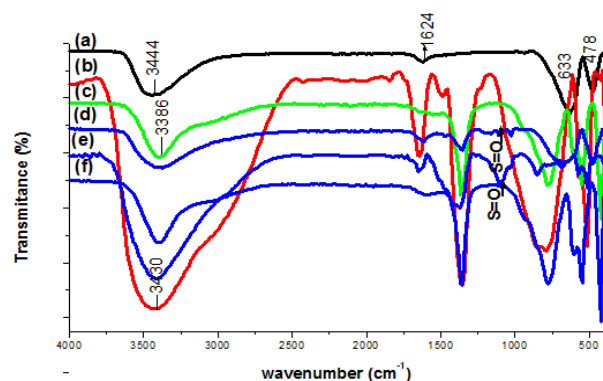


Figure 2. FTIR spectra of: (a) Zn-Fe- CO_3 , (b) Zn-Cr- CO_3 , (c) Zn-Al- CO_3 / (d), (e) and (f) for Zn-Fe- CO_3 , Zn-Cr- CO_3 and Zn-Al- CO_3 , respectively after IC adsorption.

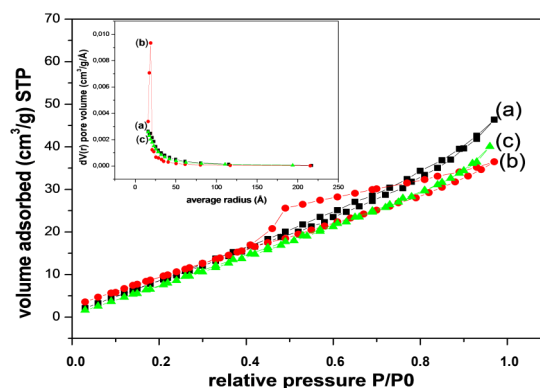


Figure 3. Nitrogen adsorption-desorption isotherm at 77.4 K and BJH pore size distribution inset for: (a) Zn-Fe- CO_3 , (b) Zn-Cr- CO_3 , (c) Zn-Al- CO_3

Table 2. Unit cell parameters and interlamellar distance of LDHs

Sample	a (Å)	c (Å)	Interlamellar distance (Å)
Zn-Al- CO_3	3.06	22.56	7.52
Zn-Cr- CO_3	3.10	22.98	7.66
Zn-Fe- CO_3	3.13	23.34	7.78

groups in the layers ($\text{Zn}/\text{M}^{+3}\text{-OH}$ or Zn-OH) and the presence of water molecules between layers [38]. The adsorption band in the range $1650\text{--}1600\text{ cm}^{-1}$ is due to the bending vibration of the interlayer water molecules [35], centered at 1642 cm^{-1} for Zn-Cr-CO_3 and it is not apparent in the case of Zn-Fe-CO_3 and Zn-Al-CO_3 , the sharp absorption bands located around 1624 , 1356 and 1359 cm^{-1} can be attributed to the anti-symmetric stretching vibrations of carbonate anions for the Zn-Fe-CO_3 , Zn-Cr-CO_3 , and Zn-Al-CO_3 samples [37–39]. A series of bands in the range of $1000\text{--}400\text{ cm}^{-1}$ corresponded to the existence of lattice translational modes (Zn-OH) and vibrational modes of the lattice showing the Zn-O , $\text{M}^{+3}\text{-O}$, O-Zn-O , or $\text{O-M}^{+3}\text{-O}$ bonds while the weak bands around 633 , 750 , and 800 cm^{-1} were assigned to unidentate carbonate symmetric stretching vibrations (O-C-O bond) for Zn-Fe-CO_3 , Zn-Cr-CO_3 , and Zn-Al-CO_3 LDHs [37–39]. The vibration bands associated with the organic anion, as well as the adsorption bands characteristic for our samples after IC adsorption are evidenced in the spectrum (d), (e) and (f), the asymmetric stretching vibration related to the S=O bond appears between $1000\text{--}1125\text{ cm}^{-1}$. The adsorption bands at around 1360 and 1620 cm^{-1} are assigned to the stretching vibration of the C=C bond belonging to an aromatic ring, while the bands at 1635 and 1065 cm^{-1} are assigned to those of C=O and C-N bond respectively [40], the band characteristic to the carbonate anion is evidenced with a considerable decrease in intensity shown in spectrum (e) compared with spectrum (b), confirms the fact that the interlayer carbonate anions have been displaced [41]. In the light of these results, we can deduce that the structural differences between the obtained products were thus confirmed from the results of FTIR meas-

urements, and these results were consistent with those of powder XRD analyses. FTIR spectra show that the uptake of IC can be done with our samples.

3.1.3 Surface area measurements

The isotherms of nitrogen adsorption-desorption at 77.4 K for Zn-Fe-CO_3 , Zn-Cr-CO_3 and Zn-Al-CO_3 are shown in Figure 3. In set of that figures is presented the BJH pore size distribution for each sample and the results of surface area measurements are included in Table 3. According to International Union of Pure and Applied Chemistry Association (IUPAC) classification [42], is noted that the Zn-Fe-CO_3 , and Zn-Al-CO_3 isotherms are of type IV and type II for Zn-Cr-CO_3 . Desorption started immediately after completion of the adsorption Figure 3(a) and 3(c) which show hysteresis loop in the middle and high-pressure region of the curve, a large uptake of nitrogen is observed close to the saturation pressure Figure 3(b), exhibiting multilayer adsorption and implying the presence of mesopores [43]. The slight changes in the hysteresis loops were observed for our samples, due to the nature of trivalent cation, these changes are related to the shape and homogeneity of the pore size Figure 3. Furthermore, the pore-size distribution curves of each samples were calculated according to the Barrett, Joyner and Halenda (BJH) method [34] were vary between 2 nm and 50 nm diameter, indicating the mesoporous structure of these samples. The sample Zn-Fe-CO_3 , whose textural characteristics are given in the Table 3, seems to have the best adsorption properties. Indeed, it exhibits a high specific surface area of about $52.24\text{ m}^2\cdot\text{g}^{-1}$ and a large porous volume of about $0.071\text{ cm}^3\cdot\text{g}^{-1}$.

3.2 Adsorption Behavior

3.2.1 Effect of initial pH on dye adsorption

As it is known, in any adsorption study, the optimization of the adsorption capacity as a function of pH is necessary in order to specify

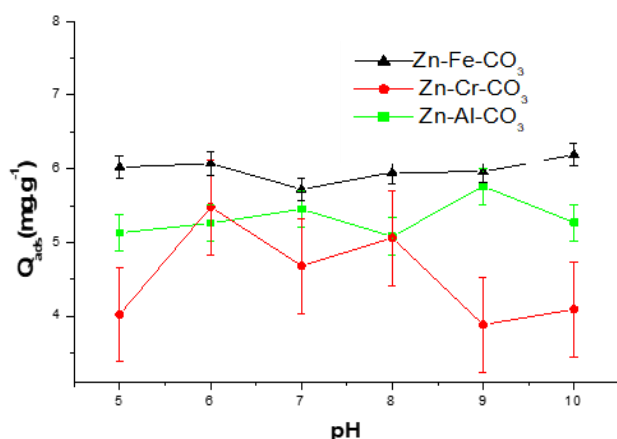


Figure 4. Effect of initial pH solution on the dye removal with errors bars

Table 3. Textural properties of LDHs

Sample	S_{BET}	V_p	D_p
Zn-Al-CO ₃	49.99	0.061	25.98
Zn-Cr-CO ₃	46.70	0.056	28.96
Zn-Fe-CO ₃	52.24	0.071	29.66

S_{BET} : Specific surface area ($\text{m}^2\cdot\text{g}^{-1}$)

V_p : Cumulative pore volume ($\text{cm}^3\cdot\text{g}^{-1}$)

D_p : Pore diameter (nm)

the pH range for which adsorption by LDHs is effective and optimal. Keeping this in view, the removal of IC dye (50 mg.L⁻¹) at different pH values ranging from 5 to 10 onto Zn-Fe-CO₃, Zn-Cr-CO₃ and Zn-Al-CO₃ layered double hydroxides were studied, the adsorption of IC is still effective within this range (Figure 4). Following these experiments, it was decided to carry out the retention experiments at pH of the solution (pH= 5.3). Furthermore, improving the removal efficiency of IC by changing the range of pH from 2 to 12 should be further investigated in future.

3.2.2 Effect of contact time on dye adsorption

Effect of sorption time on IC removal by our samples is shown in Figure 5. Adsorption at different contact time were studied using optimum adsorbents dose of 0.06 g of each solid keeping all other parameters constant. The first observation indicates that the quantity of dye adsorbed increased rapidly within the first 55, 40, and 15 minutes for Zn-Al-CO₃, Zn-Cr-CO₃, and Zn-Fe-CO₃, respectively and its rate slowed down as the equilibrium approach. According to several authors [44-45], the adsorption can be controlled by the transferring step of the adsorbate through the outer liquid film and/or of the diffusion of the solute within the adsorbent particle. The adsorbed amounts of dye was found to increase from 3.74, 5.83, and 5.9 mg.g⁻¹, respectively for Zn-Cr-CO₃, Zn-Al-CO₃ and Zn-Fe-CO₃. Despite the fact that the specific surface area of Zn-Al-CO₃ is higher than that of Zn-Cr-CO₃ but the interlayer spacing of Zn-Cr-CO₃ was found larger than that of

Zn-Al-CO₃ as confirmed by PXRD. The affinity of IC dye towards Zn-Al-CO₃ and Zn-Cr-CO₃, respectively, which confirms that the process only involves adsorption on materials surface.

The kinetic data are further utilized in the kinetic modeling to estimate the rate constants along with the removal capacity of these materials. Pseudo-first-order derived by Lagergren Equation (6) [46] and pseudo-second-order model suggested by Ho & McKay Equation (7) [47].

$$\frac{1}{Q_t} = \left(\frac{k_1}{Q_e}\right)\left(\frac{1}{t}\right) + \frac{1}{Q_e} \quad (6)$$

$$\frac{t}{Q_t} = \frac{1}{k_2 Q_e^2} + \frac{1}{Q_e} t \quad (7)$$

where Q_t is the amount of IC sorbed (mg.g⁻¹) at a given time t , Q_e the maximum adsorption capacity (mg.g⁻¹), k_1 and k_2 the pseudo-first-order and pseudo-second-order rate constants, respectively. The calculated parameters of the pseudo-first-order and pseudo second-order models IC sorption by Zn-Al-CO₃, Zn-Cr-CO₃ and Zn-Fe-CO₃ LDHs were estimated with the aid of a linear regression. The obtained data and the correlation coefficients, R^2 , are given in Table 4.

As shown in Figure 6 and Table 4, the high correlation coefficients for the pseudo-second-order model (0.99), as were the low values of Δq , χ^2 and $RMSE$, suggested that the adsorption process followed pseudo-second-order kinetic model. Furthermore, the difference between the calculated Q_e obtained from pseudo-

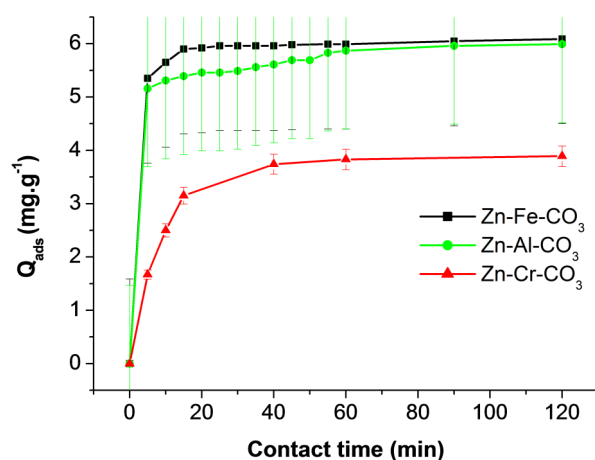


Figure 5. Effect of contact time on the adsorption of IC by Zn-Fe-CO₃, Zn-Cr-CO₃ and Zn-Al-CO₃ (pH = 5.3, V = 200 mL, C_i = 20 mg/L, T = 25 °C) with errors bars.

Table 4. Kinetic parameters and regression coefficients (R^2) for the two kinetic models.

Parameter	Zn-Cr-CO ₃	Zn-Al-CO ₃	Zn-Fe-CO ₃
First order model	Q_{exp} (mg.g ⁻¹)	3.74	5.68
	k_1 (min ⁻¹)	13.91	2.20
	Q_e (mg.g ⁻¹)	6.12	6.55
	R^2	0.90	0.36
	χ^2	24.06	2.42
	Δq	1.49	0.18
	RMSE	3.09	0.37
Second order model	Q_{exp} (mg.g ⁻¹)	3.74	5.68
	k_2 (g.mg ⁻¹ .min ⁻¹)	0.048	0.10
	Q_e (mg.g ⁻¹)	4.20	5.97
	R^2	0.99	0.99
	χ^2	5.45	0.49
	Δq	0.76	0.084
	RMSE	1.34	0.43

second-order kinetic equation and the experimental Q_{exp} was small, meaning that the pseudo-second-order kinetic model was reasonable. As may be seen that the pseudo-second-order model was better than the Lagergren first-order model for the systems investigated in this experience, the good fit with experimental data for all samples confirm that the velocity control mechanism of adsorption is chemical adsorption. A similar phenomenon is observed in the adsorption of methyl orange onto Zn-Al layered double hydroxides [30].

3.2.3 Adsorption isotherms

Experimental isotherm data of IC adsorption onto LDHs are displayed in Figure 7. The capacity of adsorption Q_e increase with the rise of dye concentration C_e until reaching an equilibrium that corresponded to the maximum of adsorption for which the surface of adsorption

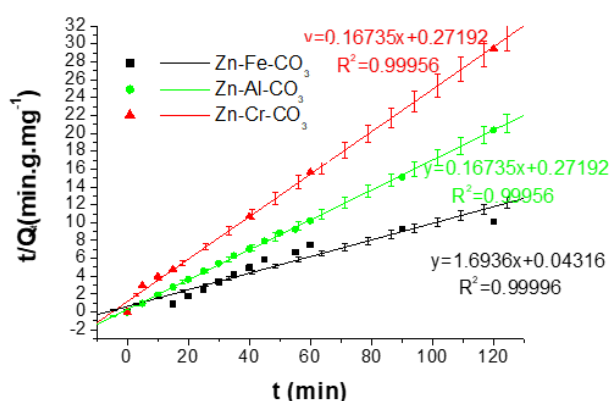


Figure 6. Adsorption of dye onto Zn-Fe-CO₃, Zn-Cr-CO₃, and Zn-Al-CO₃: 2nd order kinetic model with errors bars.

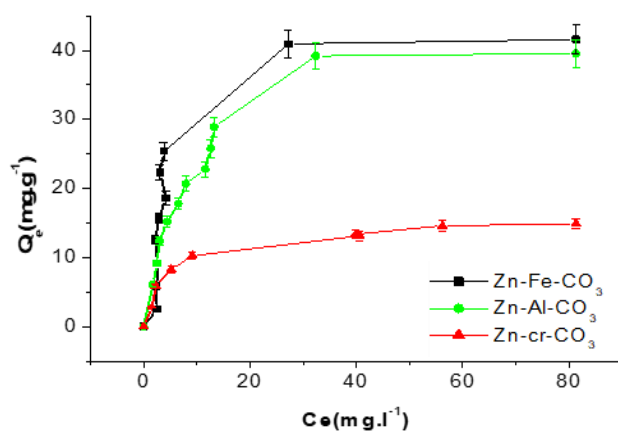


Figure 7. Adsorption isotherm of IC onto Zn-Fe-CO₃, Zn-Cr-CO₃, and Zn-Al-CO₃ LDHs ($m=0.06$ g, $pH=5.3$, $V=20$ mL, contact time = $t_{optimal}$, $T=25$ °C) with errors bars

is saturated. It can be observed that all isotherms curves display the typical “L” shape according to the classification of Giles [48]. The maximum amount of adsorption obtained are 21.79, 66.71, and 94.87 mg.g⁻¹ of IC for Zn-Cr-CO₃, Zn-Al-CO₃, and Zn-Fe-CO₃, respectively.

Several models have been used in the adsorption studies to describe the experimental data adsorption isotherms. In this work, Langmuir and Freundlich isotherm models were evaluated. The Langmuir adsorption model [49] is based on the assumption that the maximum adsorption corresponds to a saturated monolayer of solute molecules on the adsorbent surface. The adsorption data have been fitted to Langmuir adsorption model to estimate the maximum adsorption capacity Q_{max} correlated to the complete monolayer coverage of the sorbent surface. The equation is given as:

$$Q_e = \frac{Q_{max} b C_e}{1 + b C_e} \quad (8)$$

By taking the reciprocal of Equation (8), the linear form is given by Equation (9):

$$\frac{1}{Q_e} = \frac{1}{Q_{max} b C_e} + \frac{1}{Q_{max}} \quad (9)$$

where Q_e (mg.g⁻¹) is the amount of dye removed per gram of sorbent, Q_{max} (mg.g⁻¹) is the maximum adsorption capacity, C_e (mg.g⁻¹) is the dye concentration in the equilibrium solution, and b (L.mg⁻¹) is the Langmuir constant related to the affinity of the binding sites. When the surface of the LDHs is saturated with the dye, Q_m and b were determined from the linear plot of $1/Q_e$ versus $1/C_e$.

The Freundlich isotherm [50] is purely empirical and known to be satisfactory for low concentration is expressed by the Equation (10):

$$Q_e = k_F \times C_e^{1/n} \quad (10)$$

The Freundlich parameters are determined using the linear form of this model, by Equation (11):

$$\log Q_e = \frac{1}{n} \log C_e + \log k_F \quad (11)$$

where k_F and n are the Freundlich parameters, whose values were obtained from the plot of $\log Q_e$ against $\log C_e$. The linear form of Langmuir is given in Figure 8. The determined Langmuir and Freundlich parameters are tabulated in Table 5.

By comparing the values of R^2 , χ^2 , Δq , $RMSE$ (Table 5), the best fit of experimental data was obtained with the Langmuir model, indicating the homogeneous nature of all the surfaces and the formation of a monolayer of IC molecules on the surface of the adsorbents. The adsorption capacities decreased in the following order: $\text{Zn-Fe-CO}_3 > \text{Zn-Al-CO}_3 > \text{Zn-Cr-CO}_3$. This behaviour can be attributed to the peculiar structural properties of each LDHs. As confirmed by BET, the surface area decreased in the same order.

3.3 TG and DSC Analyses

The TG and DSC curves for Zn-Fe-CO_3 , Zn-Fe-IC and pure IC are illustrated in Figure 9. The results are obtained in the form of the decay curves of the mass associated with the DSC peaks as a function of temperature where the thermogram of $[\text{Zn-Fe-IC}]$ is different from that of $[\text{Zn-Fe-CO}_3]$, which confirms the retention of IC. The thermal evolution under air take place in five consecutive mass loss for which the inflexion points coincide with temperatures corresponding to minima and maxima in the DSC. The first loss of mass from about 26% to 225 °C, to this loss of mass is associated two endothermic peaks at 120 °C and 225 °C correspond to loss of physically adsorbed water and water in the interfoliar space.

In the range 225-600 °C, the loss of mass 3% is a combination of decarbonation and dehydroxylation of the material, this destruction takes place at the same temperature range as that for the parent material $[\text{Zn-Fe-CO}_3]$ 525 °C. This can be explained by the large interfoliar distance after dye adsorption. A crystallization peak appeared at 425 °C as an exothermic event due to the formation of mono-oxides.

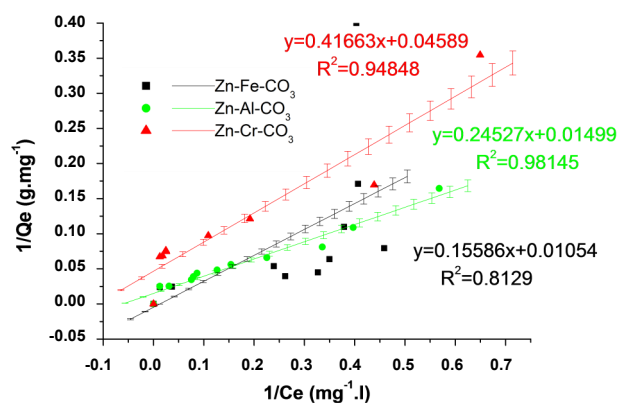


Figure 8. Linear plot of adsorption isotherm of IC dye onto Zn-Fe-CO_3 , Zn-Cr-CO_3 , and Zn-Al-CO_3 LDHs according to the Langmuir model with errors bars.

For free IC, it is noticed that two sharp exothermic peaks at 450 °C and 600 °C, these two same peaks were obtained in a higher temperature for the encapsulated IC. The LDHs stabilizes IC and delays the combustion of adsorbed molecules. As well, after 600 °C the mass loss is low when the dye is retained, coinciding with endothermic peak in the DSC profile, it probably corresponds to the elimination of a fragment, which contains sulphur in the form of SO_2 because of its slow diffusion in the oxide matrix [51], an exothermic peak due to crystallization and the formation of mixed oxides,

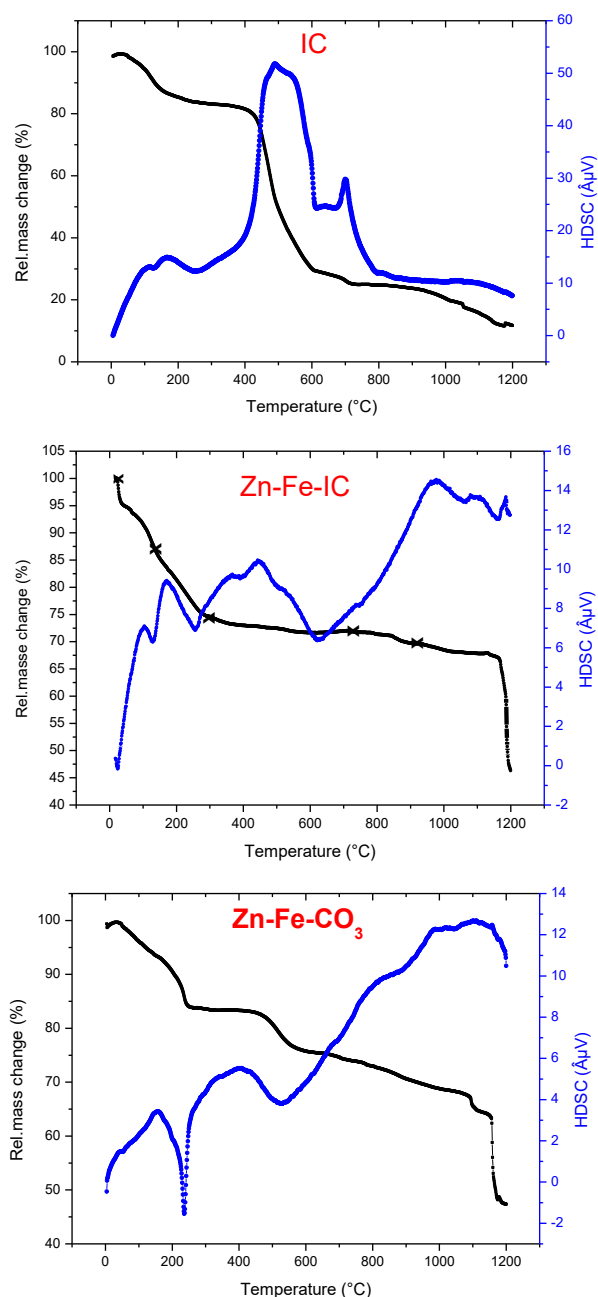


Figure 9. ATG and DSC curves obtained for pure IC, $[\text{Zn-Fe-IC}]$, and $[\text{Zn-Fe-CO}_3]$

ZnO, ZnFe₂O₄, Fe₃O₄, and Fe₂O₃, as shown in Figure 10. Similar phenomenon are previously reported for hydrotalcite-like materials [52].

4. Conclusion

This study evaluated the effect of Fe³⁺, Cr³⁺, and Al³⁺ as trivalent cations on the physico-chemical properties and dye removal by layered double hydroxides intercalated by CO₃²⁻. We were successful to prepare a novel pure Zn-Fe-CO₃ LDHs prepared from zinc and iron(II) precursors with a Zn/Fe molar ratio of 1:1. The XRD patterns display high crystallinity of Zn-Fe-CO₃ and showed that the interlayer spacing followed this order: Zn-Fe-CO₃ > Zn-Cr-CO₃ > Zn-Al-CO₃. BET surface area of Zn-Fe-CO₃ was higher than Zn-Cr-CO₃ and Zn-Al-CO₃. FTIR analysis after adsorption of IC showed the presence of the vibration bands associated with the organic anion in the interlayer region, indicating that the IC could be adsorbed on our samples. The equilibrium adsorption was increased by increasing the initial dye concentration in the solution. Adsorption kinetics data fitted well to a pseudo second-order kinetic model. The study shows that the results fit well the Langmuir model and the adsorbents used displays a high adsorption capacity of 21.79, 66.71 and 94.87 mg.g⁻¹ for Zn-Cr-CO₃, Zn-Al-CO₃, and Zn-Fe-CO₃, respectively. The results indicated that the adsorption capacities were slightly influenced by the pH variations from 5 to 10, showing the advantage of using these materials in water treatments in a wide pH range. ATG/DSC analysis of Zn-Fe-CO₃ after adsorption indicates that the LDHs stabilizes IC and delays the combustion of adsorbed molecules. In addition, the final product is a mixture of oxides that may be used as catalysts.

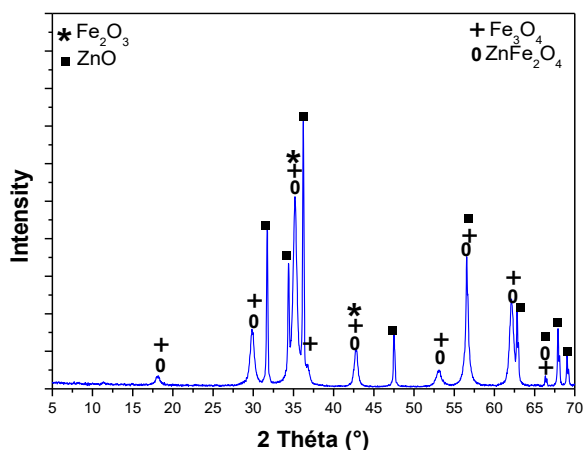


Figure 10. XRD pattern of [Zn-Fe-IC] calcined at 700 °C.

Acknowledgements

Some analyses were performed at the LCSCO UABT (Tlemcen, Algeria), the laboratory members (Laboratory of Inorganic Materials Chemistry and Application (LCMIA), University of Sciences and Technology of Oran, Algeria) are kindly acknowledged for their contribution to this work.

References

- [1] Itoh, K., Kitade, Y., Yatote, C. (1996). A pathway for biodegradation of an anthraquinone dye, C. I. disperse red 15, by a yeast strain *pichia anomala*. *Bull. Environ. Contam. Toxicol.*, 56: 413-418.
- [2] Pinherio, H.M., Touraud, E., Tomas, O. (2004). Aromatic amines from azo dye reduction: status review with emphasis on direct UV spectrophotometric detection in textile industry wastewater. *Dyes Pigm.*, 61: 121-139.
- [3] Barka, N., Qourzal, S., Assabbane, A., Nounah, A., Ait-Ichou, Y. (2011). Triphenylmethane Dye, Patent Blue V, Photocatalytic Degradation on Supported TiO₂: Kinetics, Mineralization and Reaction Pathway. *Chem. Eng. Commun.*, 198: 1233-1243.
- [4] Suzuki, T., Timofei, S., Kurunczi, L., Dietze, U., Schuurmann, G. (2001). Correlation of aerobic biodegradability of sulfonated azo dyes with the chemical structure. *J. Chromatogr.*, 45: 1-9.
- [5] Yichen, H., Xiao, C., Zhiqiang, L., Gejiao, W., Shuijiao, L. (2016). Activated carbon doped with biogenic manganese oxides for the removal of indigo carmine. *J. Environ. Manage.*, 166: 512-518.

Table 5. Freundlich and Langmuir constants for IC adsorption onto Zn-Fe-CO₃, Zn-Cr-CO₃, and Zn-Al-CO₃ LDHs.

Parameters	Zn-Cr-CO ₃	Zn-Al-CO ₃	Zn-Fe-CO ₃
Freundlich	k_F	2.34	3.71
	n	2.05	1.40
	R^2	0.88	0.86
	χ^2	72.33	206.31
	Δq	0.2273	0.54
	RMSE	4.20	14.16
Langmuir	Q_{max} (mg.g ⁻¹)	21.79	66.71
	b	0.110	0.061
	R^2	0.94	0.98
	χ^2	2.73	79.95
	Δq	0.0539	0.0034
	RMSE	1.66	14.0408

- [6] Khadhri, N., Mohamed El Khames, S., ben Mosbah, M., Moussaoui, Y. (2019). Batch and continuous column adsorption of indigo carmine onto activated carbon derived from date palm petiole. *J. Environ. Chem. Eng.*, 7: 102775.
- [7] Mustafa, B., Kaan, B., Bengisu, Y., Melih, P., Yuda, Y. (2018). Preparation of high surface area activated carbon from waste-biomass of sunflower piths: Kinetics and equilibrium studies on the dye removal. *Environ. Chem. Eng.*, 6(2): 1702-1713.
- [8] El Khames Saad, M., Mnasri, N., Mhamdi, M., Tarik, C., Elimame, E., Moussaoui, Y. (2015). Removal of methylene blue onto mineral matrices. *Desalin. Water Treat.*, 56: 2773-2780.
- [9] Kachbouri, S., Mnasri, N., Elimame, E., Moussaoui, Y. (2018). Tuning particle morphology of mesoporous silica nanoparticles for adsorption of dyes from aqueous solution. *J. Saudi Chem. Soc.*, 22: 405-415.
- [10] Santos, A.B.D., Cervantes, F.J., Lier, J.B.V. (2007). Review paper on current technologies for decolourisation of textile wastewaters: perspectives for anaerobic biotechnology. *Bio-resour. Technol.* 98: 2369-2385.
- [11] Ouanji, F., Ellouzi, I., Kacimi, M., Ziyad, M. (2019). Ca-hydroxyzincate: Synthesis and Enhanced Photocatalytic Activity for the Degradation of Methylene Blue Under UV-Light Irradiation. *Chem. Africa*, 2(3), 395-400.
- [12] Sureshkumar, M.V., Namasivayam, C. (2008). Adsorption Behavior of Direct Red 12B and Rhodamine B From Water Onto Surfactant-Modified Coconut Coir Pith. *Colloids Surf. A: Physicochem. Eng. Aspects*, 317: 277-283.
- [13] Alventosa-deLara, E., Barredo-Damas, S., Zuriaga-Agustí, E., Alcaina-Miranda, M.I., Iborra-Clar, M.I. (2014). Ultrafiltration ceramic membrane performance during the treatment of model solutions containing dye and salt. *Purif.*, 129: 96-105.
- [14] Ravikumar, K., Krishnan, S., Ramalingam, S., Balu, K. (2007). Optimization of Process Variables by the Application of Response Surface Methodology for Dye Removal Using a Novel Adsorbent. *Dyes Pigm.*, 72: 66-74.
- [15] Li, Y., Zhou, K., He, M., Yao, J. (2016). Synthesis of ZIF-8 and ZIF-67 using mixed-base and their dye adsorption. *J. Micropor. Mesopor. Mat.*, 234: 287-292.
- [16] Lakraimi, M., Legrouri, A., Barroug, A., De Roy, A., Besse, J.P. (2000). Preparation of a new stable hybrid material by chloride-2,4-dichlorophenoxyacetate ion exchange into the zinc-aluminium-chloride layered double hydroxide. *J. Mater. Chem.*, 10: 1007-1011.
- [17] Sillion, M., Dobrea, I.D., Nistor, D., Popa, M.I. (2013). Environmentally friendly formulations of 2,6-dichlorobenzonitrile pesticide intercalated into calcined layered double hydroxides. *Environ. Eng. Manag. J.*, 12: 2465-2471.
- [18] Chowdhury, P.R., Bhattacharya, K.G. (2015). Ni/Ti layered double hydroxide: synthesis, characterization and application as a photocatalyst for visible light degradation of aqueous methylene blue. *Dalton Trans.*, 44: 6809-6824.
- [19] Zhang, Z., Kong, J. (2011). Novel magnetic Fe₃O₄ nanoparticles as adsorbents for removal of organic dyes from aqueous solution. *J. Hazard. Mater.*, 193: 325-329.
- [20] Ai, L., Zhang, C., Liao, F., Wang, Y., Li, M., Meng, L., Jiang, J. (2011). Removal of ethyleneblue from aqueous solution with magnetite loaded multi-wall carbonnanotube: kinetic, isotherm and mechanism analysis. *J. Hazard. Mater.*, 198: 282-290.
- [21] Fan, L., Luo, C., Li, X., Lu, F., Qiu, H., Sun, M. (2012). Fabrication of novel magnetic chitosangrafted with graphene oxide to enhance adsorption properties for methyl blue. *J. Hazard. Mat.*, 215-216: 272-279.
- [22] Sahu, R.K., Mohanta, B.S., Das, N.N. (2013). Synthesis, characterization and photocatalytic activity of mixed oxides derived from ZnAl-Ti ternary layered double hydroxides. *J. Phys. Chem. Solids*, 74: 1263-1270.
- [23] Toledo, T.V., Bellato, C.R., Pessoa, D.K., Fontes, M.P.F. (2013). Removal of chromium (VI) from aqueous solutions using the calcined magnetic composite hydrotalcite-iron oxide: kinetic and thermodynamic equilibrium studies. *Quím. Nova.*, 36: 419-425.
- [24] Miranda, L.D.L., Bellato, C.R., Fontes, M.P.F., De Almeida, M.F., Milagres, J., Minim, L.A. (2014). Preparation and evaluation of hydrotalcite-iron oxide magnetic organo composite intercalated with surfactants for cationic methylene blue dye removal. *Chem. Eng.*, 254: 88-97.
- [25] Joseph, W.B., Paul, S.B., Jiang, J., Lou, S., Yarberry, F. (1999). Layered double hydroxide stability. 1. Relative stabilities of layered double hydroxides and their simple counter parts. *Chem. Mater.*, 11: 303-307.
- [26] Newman, S.P., Jones, W. (1998). Synthesis, characterization and application of layered double hydroxide containing organic guests. *New J. Chem.*, 22: 105-115.
- [27] Reichle, W.T. (1986). Synthesis of anionic clay minerals (mixed metal hydroxides, hydrotalcite). *Solid State Ionics*, 22: 135-141.

- [28] Kannan, S., Swamy, S. (1997). Effect of trivalent cation on the physicochemical properties of cobalt containing anionic clays. *J. Mat. Sci.*, 32(6): 1623-1630.
- [29] Rojas, R. (2012). Layered double hydroxides applications as sorbents for environmental. *Nova Science Publisher*. Chapter 2
- [30] Mahjoubi, F.Z., Khalidi, A., Cherkaoui, O., Elmoubarki, R., Abdennouri, M., Barka, N. (2017). Treatment of textile effluents by chloride-intercalated Zn-, Mg- and Ni-Al layered double hydroxide. *J. Water. Reuse. Desal.*, 7: 307-318.
- [31] Morimoto, K., Tamura, K., Anraku, S., Sato, T., Suzuki, M., Yamada, H. (2015). Synthesis of Zn-Fe layered double hydroxides via an oxidation process and structural analysis of products. *J. Solid State Chem.*, 228: 221-139.
- [32] Meng, W., Li, F., Evans, D.G., Duan, X. (2004). Photocatalytic activity of highly porous zinc ferrite prepared from a zinc-iron(III)-sulfate layered double hydroxide precursor. *J. Porous. Mat.*, 11: 97-105.
- [33] JCPDS: Joint Committee on Powder Diffraction Standards, International Centre for Diffraction Data, Pennsylvania, U.S.A, (1977)
- [34] Barrett, E.P., Joyner, L.G., Halenda, P.P. (1951). The determination of pore volume and area distributions in porous substances. I. Computations from nitrogen isotherms. *J. Am. Chem. Soc.*, 73: 373-380.
- [35] Cavani, F., Trifiro, F., Vaccari, A. (1991). Hydrotalcite-type anionic clays: preparation, properties and applications. *Catal. Today*, 11: 173-301.
- [36] Shannon, R.D. (1976). Revised effective ionic radii and systematic studies of interatomic distances in halides and chalcogenides. *Acta Crystallographica Section A*, 32: 751-767.
- [37] Mohapatra, L., Parida, K.M. (2012). Zn-Cr layered double hydroxide: Visible light responsive photocatalyst for photocatalytic degradation of organic pollutants. *Sep. Purif. Tech.*, 91: 73-80.
- [38] Mahjoubi, F.Z., Khalidi, A., Abdennouri, M., Barka, N. (2017). Zn-Al layered double hydroxides intercalated with carbonate, nitrate, chloride and sulphate ions: Synthesis, characterization and dye removal properties. *J. Tai-bah Univ. Sci.*, 11: 90-100.
- [39] De Roy, A., Forano, C., Besse, J.P. (2001) Rives V. (Ed.) Nova Science, New York, NY, 1-41.
- [40] Elkhatabi, E.H., Lakraimi, M., Badreddine, M., Legrouri, A., Cherkaoui, O., Berraho, M. (2013). Removal of Remazol Blue 19 from wastewater by zinc-aluminium-chloride-layered double hydroxides. *Appl. Water. Sci.*, 3: 431-438.
- [41] Alexandrica, M.C., Silion, M., Hritcu, D., Popa1, M.I. (2015). Layered double hydroxide as adsorbents for anionic dye removal from aqueous solutions. *Environ. Eng. Manag. J.*, 14: 381-388.
- [42] Sing, K.S.W., Everett, D.H., Hall, R.A.W., Moscou, L., Pierotti, R.A., Rouqu  rol, J., Siemieniewska, T. (1985). IUPAC Recommendations 1984. *Pure. Appl. Chem.*, 57(4): 603-619.
- [43] Wang, C.C., Juang, L.C., Lee, C.K., Hsu, T.C., Lee, J.F., Chao, H.P. (2004). Effect of exchanged surfactant cations on the pore structure and adsorption characteristics of montmorillonite. *J. Colloid Interface Sci.*, 280: 27-35.
- [44] Tragn  g, U.K., Suiclan, M.T. (1989). Evaluation of surface and film diffusion coefficients for carbon adsorption. *Water. Res.*, 23: 267-273.
- [45] Belmouden, M., Assabbane, A., Ait-Ichou, Y. (2000). Adsorption characteristics of a phenoxy acetic acid herbicide on activated carbon. *J. Environ. Monit.*, 2: 257-260.
- [46] Lagergren, S. (1998). About the theory of so-called adsorption of soluble substance. *H  ndlingar*, 16: 1-39.
- [47] Ho, Y.S., McKay, G. (1999). Pseudo-Second Order Model for Sorption Processes. *Process Biochem.*, 34: 451-465.
- [48] Giles, C.H., Macewan, T.H., Nakhwa, S.N., Smit, D. (1960). Studies in Adsorption: Part XI. A System of Classification of Solution Adsorption Isotherms and Its Use in Diagnosis of Adsorption Mechanisms and in Measurement of Specific Surface Area Solids. *J. Chem. Soc.*, 14: 3973-3993.
- [49] Langmuir, I. (1916). The constitution and fundamental properties of solids and liquids. *Journal of the American Chemical Society*, 38: 2221-2295.
- [50] Freundlich, H.M.F. (1906). Uber die adsorption in losungen. *Journal of Physical Chemistry*, 57: 385-470.
- [51] Lakraimi, M., Legrouri, A., Barroug, A., De Roy, A., Besse, J.P. (2006). Synthesis and characterization of a new stable organo-mineral hybrid nanomaterial: 4-chlorobenzenesulfonate in the zinc-aluminium layered double hydroxide. *Mater. Res. Bull.*, 41: 1763-1774.
- [52] Elkhatabi, E.H., Lakraimi, M., Berraho, M., Legrouri, A., Hammal, R., El Ghaini, L. (2018). Acid Green 1 removal from wastewater by layered double hydroxides. *App. Water Sci.*, 8: 1-11.